
Precursors and prediction of catastrophic avalanches

Srutarshi Pradhan¹ and Bikas K. Chakrabarti²

¹ Norwegian University of Science and Technology, Trondheim, Norway

`pradhan.srutarshi@ntnu.no`

² Saha Institute of Nuclear Physics, Kolkata, India

`bikask.chakrabarti@saha.ac.in`

1 Introduction

In this chapter we review the precursors of catastrophic avalanches (global failures) in several failure models, namely (a) Fiber Bundle Model (FBM), (b) Random Fuse Model (RFM), (c) Sandpile Models and (d) Fractal Overlap Model. The precursor parameters identified here essentially reflect the growing correlations within such systems as they approach their respective failure points. As we show, often they help us to predict the global failure points in advance.

Needless to mention that the existence of any such precursors and detailed knowledge about their behavior for major catastrophic failures [1] like earthquakes, landslides, mine/bridge collapses, would be of supreme value for our civilization. So far, we do not have any established set of models for these major failure phenomena. However, several reasonable models of failure have already been developed in various contexts. We review here some of the precursors of global failures in these models.

2 Precursors in Failure models

2.1 Composite material under stress: Fiber bundle model

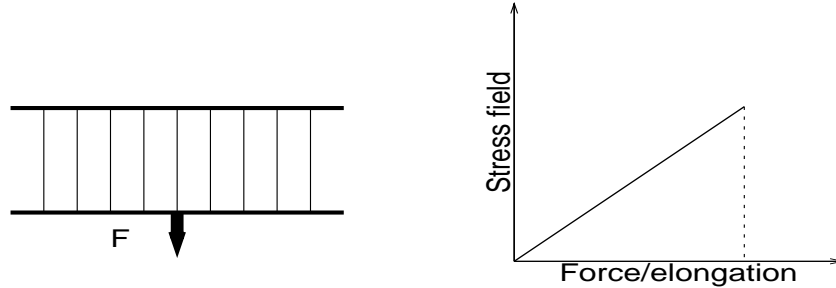


Fig. 1: Fiber bundle model (left) and the force-response of a single fiber (right).

Fiber bundle model represents various aspects of fracture-failure process in composite materials. A bundle of parallel fibers, clamped at both ends (Fig. 1 (left)) represents the model where fibers are assumed to obey Hookean elasticity up to the breaking point (Fig. 1 (right)). The model needs three basic ingredients: (a) a discrete set of N elements (b) a probability distribution of the strength of fibers (c) a load-transfer rule. Peirce [2] initiated the model study in the context of testing the strength of cotton yarns. Since then this model has been studied from different views. Fiber bundles are of two classes with respect to the time dependence of fiber strength: The ‘static’ bundles [2-10] contain fibers whose strengths are independent of time, where as the ‘dynamic’ bundles [11-13] are assumed to have time dependent elements to capture the creep rupture and fatigue behaviors. According to the load sharing rule, fiber bundles are being classified into two groups: equal load-sharing (ELS) bundles and local load-sharing (LLS). In ELS bundles, intact fibers bear the applied load equally and in LLS bundles, the terminal load of the failed fiber is given equally to all the intact neighbors. With steadily increasing load, a fiber bundle approaches the failure point obeying a dynamics determined by the load sharing rule. The phase transition [7] and dynamic critical behavior of the fracture process in such democratic bundles has been established through recursive formulation [8, 9] of the failure dynamics. The exact solutions [9, 10] of the recursion relations suggest universal values of the exponents involved. Attempts have also been made [11] to study the ELS and LLS bundles from a common framework introducing a single parameter which determines the load transfer rule.

We discuss here, failure of static fiber bundles under global load sharing (ELS) for two different loading conditions: (a) load increment by equal amount and (b) quasi-static loading -which follows weakest link failure at each step of loading. We show analytically the variation of precursor parameters with the applied stress, which help to estimate the failure point accurately.

Recursive dynamics in ELS bundle: Precursors

ELS model assumes that the intact fibers share the applied load equally. The strength threshold of a fiber is determined by the stress value it can bear, and beyond which it fails. Usually, thresholds are taken from a randomly distributed normalised density $p(x)$ within the interval 0 and 1 such that

$$\int_0^1 p(x)dx = 1. \quad (1)$$

The breaking dynamics starts when an initial stress σ (load per fiber) is applied on the bundle. The fibers having strength less than σ fail instantly. Due to this rupture, total number of intact fibers decreases and effective stress increases and this compels some more fibers to break. Such stress redistribution and further breaking of fibers continue till an equilibrium is reached, where either the surviving fibers are strong enough to bear the applied load on the bundle or all fibers fail.

This self organised breaking dynamics can be represented by recursion relations [8, 9] in discrete time steps. Let U_t be the fraction of fibers in the initial bundle that survive after time step t , where time step indicates the number of occurrence of stress redistribution. Then the redistributed stress after t time step becomes

$$\sigma_t = \frac{\sigma}{U_t}; \quad (2)$$

and after $t + 1$ time steps the surviving fraction of fiber is

$$U_{t+1} = 1 - P(\sigma_t); \quad (3)$$

where $P(\sigma_t)$ is the cumulative probability of corresponding density distribution $p(x)$: $P(\sigma_t) = \int_0^{\sigma_t} p(x)dx$. Now using Eq. (2) and Eq. (3) we can write the recursion relations which show how σ_t and U_t evolve in discrete time:

$$\sigma_{t+1} = \frac{\sigma}{1 - P(\sigma_t)}; \sigma_0 = \sigma \quad (4)$$

and

$$U_{t+1} = 1 - P(\sigma/U_t); U_0 = 1. \quad (5)$$

At the equilibrium or steady state $U_{t+1} = U_t \equiv U^*$ and $\sigma_{t+1} = \sigma_t \equiv \sigma^*$. This is a fixed point of the recursive dynamics. Eq. (4) and Eq. (5) can be solved at the fixed point for some particular distribution. At the fixed-point, the solutions [8, 9, 10] assume universal form

$$\sigma^*(\sigma) = C - (\sigma_c - \sigma)^{1/2}; \quad (6)$$

$$U^*(\sigma) = C + (\sigma_c - \sigma)^{1/2}; \quad (7)$$

where σ_c is the critical stress and C is a constant. From the recursions and their solutions we can derive the following response quantities:

Susceptibility: Which is defined as the amount of change in U when the external stress changes by a infinitesimal amount and can be derived as

$$\chi = \left| \frac{dU^*(\sigma)}{d\sigma} \right| = \frac{1}{2}(\sigma_c - \sigma)^{-\beta}; \beta = \frac{1}{2}. \quad (8)$$

Relaxation time: This is the number of step the bundle needs to come to a stable state after the application of an external stress. From the solution of recursive dynamics we get [8, 9] near σ_c

$$\tau \propto (\sigma_c - \sigma)^{-\theta}; \theta = \frac{1}{2}. \quad (9)$$

Inclusive avalanche: This is the amount of avalanche per step of stress redistribution

$$\frac{dU}{dt} = U_t - U_{t+1} \quad (10)$$

At $\sigma = \sigma_c$, the dynamics becomes “critically slow” as

$$U_t \sim t^{-\gamma}; \gamma = 1; \quad (11)$$

which suggests that at σ_c inclusive avalanches follow a power law (exponent -2) decay with time.

Prediction of global failure point

(A) Using χ and τ

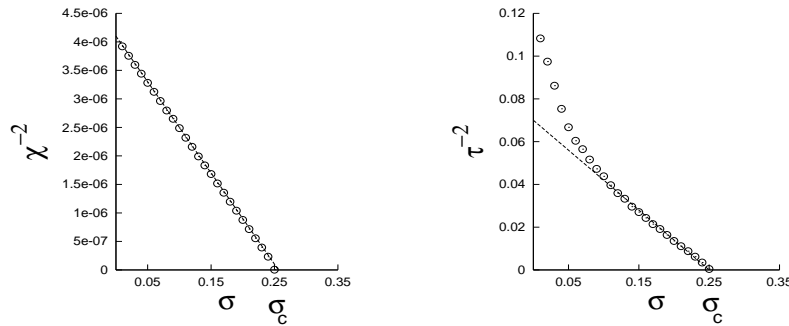


Fig. 2: Variation of χ^{-2} and τ^{-2} with applied stress for a bundle having $N = 50000$ fibers and averaging over 1000 samples. We consider uniform distribution of fiber threshold.

We found that susceptibility (χ) and relaxation time (τ) follow power laws with external stress and both of them diverge at the critical stress. Therefore if we plot χ^{-2} and τ^{-2} with external stress, we expect a linear fit near critical point and the straight lines should touch X axis at the critical stress. We indeed found similar behavior (Fig. 2) in simulation experiments.

For application, it is always important that such prediction can be done in a single sample. We have performed the simulation taking a single bundle having very large number of fibers and we observe similar response of χ and τ . The prediction of failure point is also quite satisfactory (Fig. 3).

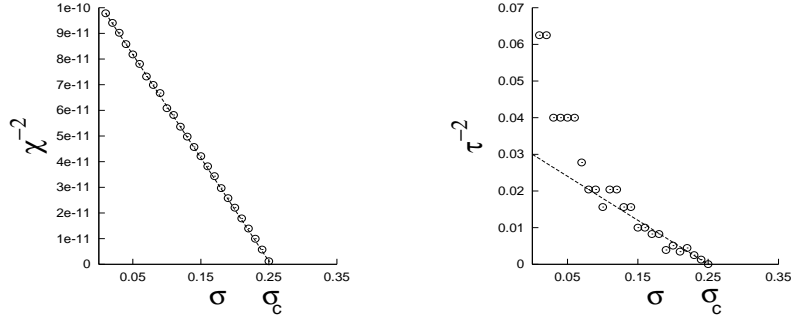


Fig. 3: Variation of χ^{-2} and τ^{-2} with applied stress for a single bundle having $N = 10000000$ fibers with uniform distribution of fiber threshold.

(B) Using inclusive avalanche

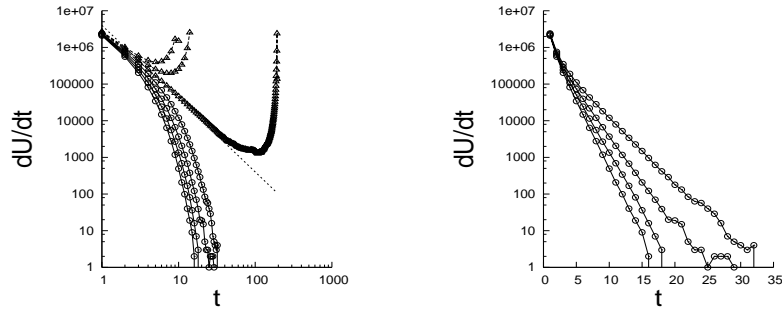


Fig. 4: Log-log plot of inclusive avalanche with step of load redistribution for 7 different stress values [left] and log-normal plot of the same for 4 different stress values below the critical stress [right]. The simulation has been performed for a single bundle with $N = 10000000$ fibers having uniform distribution of fiber threshold.

When we put a big load on a material body, sometimes it becomes important to know whether that body can support the load or not. The similar question can be asked in FBM. We found that if we record the inclusive avalanche, i.e, the amount of failure in each load redistribution -then the pattern of inclusive burst clearly shows whether the bundle is going to fail or not. For any stress below the critical state, inclusive avalanche follow exponential

decay (Fig. 4 (right)) with time step and for stress values above critical stress it is a power law followed by a gradual rise (Fig. 4 (left)). Clearly at critical stress it follows a robust power law with exponent -2 that we already get analytically.

(C) Using avalanche distribution

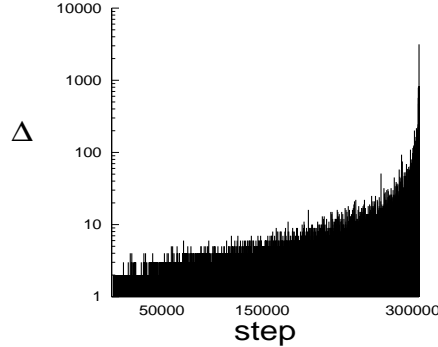


Fig. 5: Magnitude of avalanches with step of load increment in FBM.

An ‘‘Avalanche’’ is the amount of failure occurs as the system moves from one stable state to the next stable state when the load is increased quasi-statically. We can simply measure it by counting the failure elements between two consecutive load increment. Such a series of avalanches has been shown in Fig. 5 up to the final failure point. If we record all the avalanches till final failure, the avalanche distribution follows a universal power law [4]. This avalanches can be recorded experimentally measuring the acoustic emissions during fracture-failure of materials. We want to study whether the avalanche distribution changes if we start gathering the avalanches from some intermediate states of the breaking process (Fig. 6 (left)). In simulations we see that the exponent of avalanche distribution shows a crossover between two values ($-5/2$ and $-3/2$) and the crossover point (length) depends on the starting position (x_0) of our measurement (Fig. 6(right)).

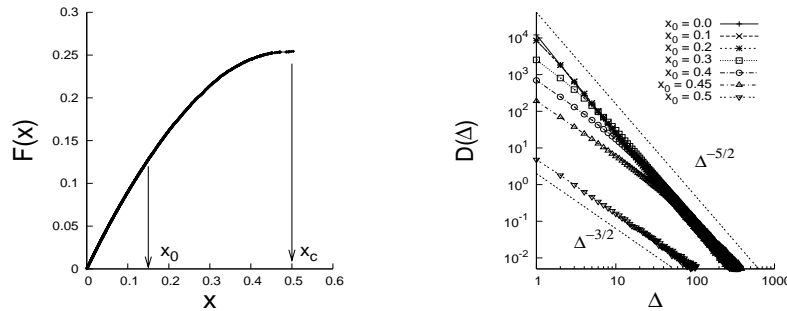


Fig. 6: Average force versus elongation curve (left) and simulation results of avalanche distributions for different starting position (right) in FBM.

Now we are going to explain the above observation analytically for quasi-static loading. For a bundle of many fibers the average number of bursts of magnitude Δ is given by [4]

$$\frac{D(\Delta)}{N} = \frac{\Delta^{\Delta-1}}{\Delta!} \int_0^{x_c} p(x) [1 - xp(x)/Q(x)] [xp(x)/Q(x)]^{\Delta-1} \quad (12)$$

$$\times \exp[-\Delta xp(x)/Q(x)] dx, \quad (13)$$

where $Q(x) = \int_x^\infty p(y) dy$ is the fraction of total fibers with strength exceeding x and x_c is the critical value beyond which the bundle fails instantly. For uniform distribution (having upper bound x_m), if we start recording avalanches from an intermediate point x_0 , the avalanche distribution becomes

$$\frac{D(\Delta)}{N} = \frac{\Delta^{\Delta-1}}{\Delta!(x_m - x_0)} \times \int_{x_0}^{x_c} \frac{x_m - 2x}{x} \left[\frac{x}{x_m - x} e^{-x/(x_m - x)} \right]^\Delta dx. \quad (14)$$

Introducing the parameter $\epsilon = \frac{x_c - x_0}{x_m}$ and a new integration variable $z = \frac{x_m - 2x}{\epsilon(x_m - x)}$, we obtain

$$\frac{D(\Delta)}{N} = \frac{2\Delta^{\Delta-1} e^{-\Delta} \epsilon^2}{\Delta!(1+2\epsilon)} \times \int_0^{4/(1+2\epsilon)} \frac{z}{(1-\epsilon z)(2-\epsilon z)^2} e^{\Delta[\epsilon z + \ln(1-\epsilon z)]} dz. \quad (15)$$

For small ϵ , i.e., close to the critical threshold distribution, we can expand

$$\epsilon z + \ln(1 - \epsilon z) = -\frac{1}{2}\epsilon^2 z^2 - \frac{1}{3}\epsilon^3 z^3 + \dots, \quad (16)$$

with the result

$$\frac{D(\Delta)}{N} \simeq \frac{\Delta^{\Delta-1} e^{-\Delta} \epsilon^2}{2\Delta!} \times \int_0^4 e^{-\Delta \epsilon^2 z^2 / 2} z dz = \frac{\Delta^{\Delta-2} e^{-\Delta}}{2\Delta!} (1 - e^{-8\epsilon^2 \Delta}). \quad (17)$$

Using Stirling approximation $\Delta! \simeq \Delta^\Delta e^{-\Delta} \sqrt{2\pi\Delta}$, this becomes

$$\frac{D(\Delta)}{N} \simeq (8\pi)^{-1/2} \Delta^{-5/2} (1 - e^{-\Delta/\Delta_c}), \quad (18)$$

with

$$\Delta_c = \frac{1}{8\epsilon^2} = \frac{x_m^2}{8(x_c - x_0)^2}. \quad (19)$$

Clearly, there is a crossover [5] at a burst length around Δ_c , so that

$$\frac{D(\Delta)}{N} \simeq \begin{cases} (8/\pi)^{1/2} \epsilon^2 \Delta^{-3/2} & \text{for } \Delta \ll \Delta_c \\ (8\pi)^{-1/2} \Delta^{-5/2} & \text{for } \Delta \gg \Delta_c \end{cases} \quad (20)$$

For $x_0 = 0.40x_m$, we have $\Delta_c = 12.5$ uniform distribution. We found a clear crossover near $\Delta = \Delta_c = 12.5$ in the simulation experiment (Fig. 7).

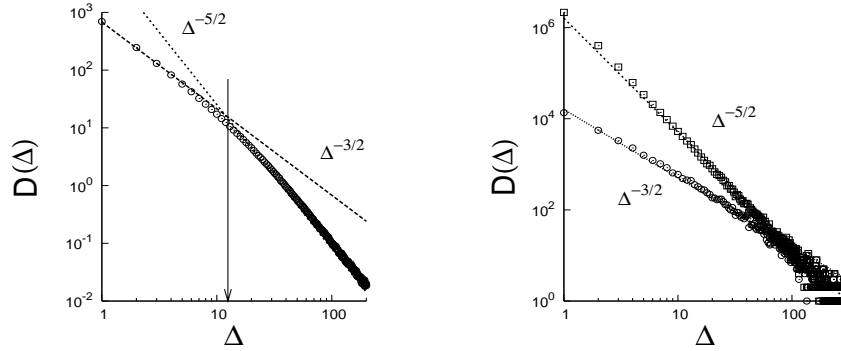


Fig. 7: Crossover in avalanche distributions: bundle with 10^6 fiber and $x_0 = 0.8x_c$ (averaging over 20000 samples) [left] and a single bundle with 10^7 fiber; $x_0 = 0$ (squares) and $x_0 = 0.9x_c$ (circles) [right]. Dotted straight lines are the best fits to the power laws.

The simulation results shown in the figures are based on *averaging* over a large number of samples. For applications it is important that crossover signals are seen also in a *single* sample. We show (Fig. 7) that equally clear power laws are seen in a *single* fiber bundle when N is large.

This crossover phenomenon is not limited to the uniform threshold distribution. The $\xi = 3/2$ power law [5] in the burst size distribution dominates over the $\xi = 5/2$ power law whenever a threshold distribution is non-critical, but close to criticality. Therefore, the magnitude of the crossover length correctly inform us how far the system is from the global failure point.

2.2 Electrical networks within a voltage difference: Random fuse model

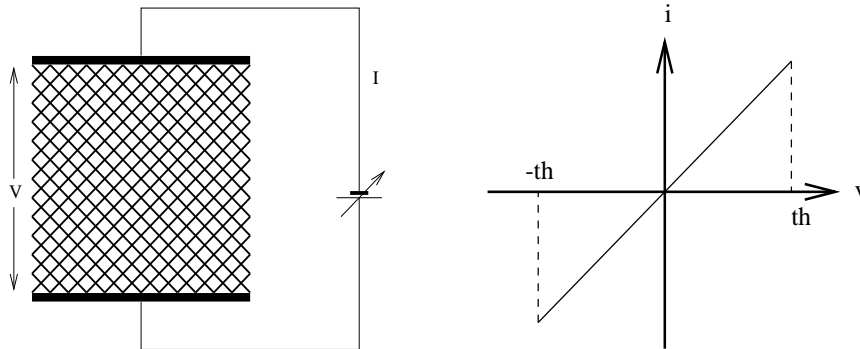


Fig. 8: Random fuse model (left) and the current-response of a single Ohmic resistor (right).

Random fuse model [1] describes the breakdown phenomena in electrical networks. It consists of a lattice in which each bond is a fuse, i.e., an Ohmic resistor as long as the electric current it carries is below a threshold value. If the threshold is passed, the fuse burns out irreversibly (Fig. 8 (right)). The threshold (th) of each bond is drawn from an uncorrelated distribution $p(th)$. All fuses have the same resistance. The lattice is a two-dimensional square one placed at 45° with regards to the bus bars (Fig. 8 (left)) and an increasing current is passed through it. Numerically, the Kirchhoff equations are solved at each point of the system.

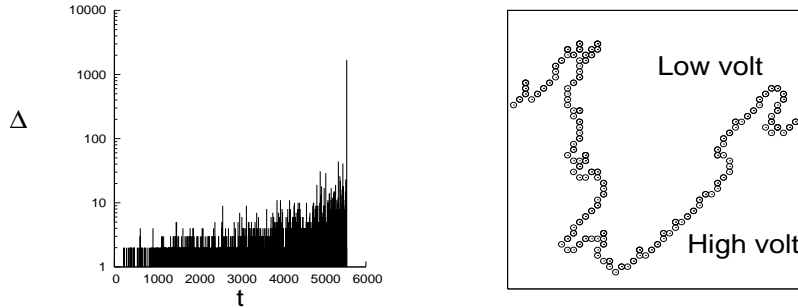


Fig. 9: Avalanches in fuse model (left) and the ultimate fractured state (right).

For the entire failure process avalanches of different sizes occur (Fig. 9 (left)) and the system finally comes to a point where no current passes through the system (Fig. 9 (right))- we call it the global failure point. The average avalanche size has been measured [7] for such system and it follows a power law with increasing current or voltage:

$$m \sim (I_c - I)^{-\gamma} \text{ or } m \sim (V_c - V)^{-\gamma}; \gamma = 1/2$$

Therefore if we plot m^{-2} with I or V we can expect a linear fit which touches X axis at the critical current value I_c or critical voltage value V_c (Fig. 10).

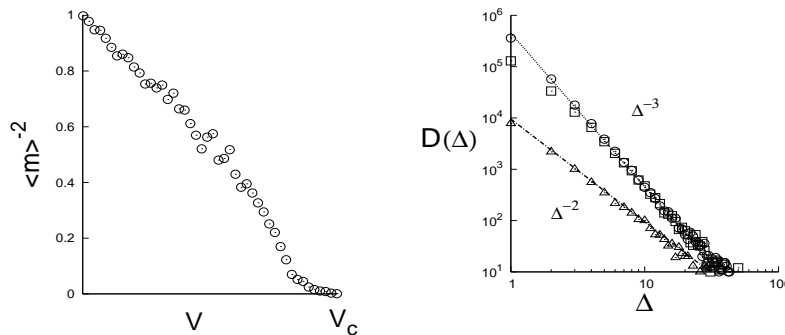


Fig. 10: Plot of m^{-2} with V (left) and the crossover in avalanche distributions in a fuse model (right).

If we record all the avalanches, the avalanche distribution follows a universal power law with $\xi \simeq 3$. But what will happen if we start recording the burst at some intermediate state of the failure process? We observe [5] that for a system of size 100×100 , 2097 fuses blow on the average before catastrophic failure sets in. When measuring the burst distribution only after the first 2090 fuses have blown, a different power law is found, this time with $\xi = 2$. After 1000 blown fuses, on the other hand, ξ remains the same as for the histogram recording the entire failure process (Fig. 10).

2.3 SOC models of sandpile

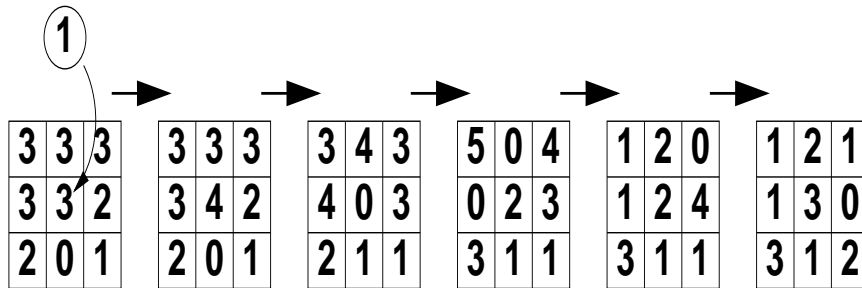


Fig. 11: A real sandpile and the sandpile model [16] on a square lattice.

Growth of a natural sandpile is a nice example of self-organised criticality [15-19]. If sand grains are added continuously on a small pile, the system gradually approaches towards a state at the boundary between stable and unstable states where the system shows long-range spatio-temporal fluctuations similar to those observed in equilibrium critical phenomena. This special state has been identified as the critical state of the pile where the response to addition of sand grains becomes unpredictable: Avalanche of any size is equally

probable at this state. Therefore, we can expect system spanning avalanche (global failure) only at this critical state.

BTW model and Manna model

Bak et. al. [15] proposed a sandpile model on square lattice which captures correctly the properties of a natural sandpile. At each lattice site (i, j) , there is an integer variable $h_{i,j}$ which represents the height of the sand column at that site. A unit of height (one sand grain) is added at a randomly chosen site at each time step and the system evolves in discrete time. The dynamics starts as soon as any site (i, j) has got a height equal to the threshold value ($h_{th} = 4$): that site topples, i.e., $h_{i,j}$ becomes zero there, and the heights of the four neighbouring sites increase by one unit

$$h_{i,j} \rightarrow h_{i,j} - 4, h_{i\pm 1,j} \rightarrow h_{i\pm 1,j} + 1, h_{i,j\pm 1} \rightarrow h_{i,j\pm 1} + 1. \quad (21)$$

If, due to this toppling at site (i, j) , any neighbouring site become unstable (its height reaches the threshold value), the same dynamics follows. Thus the process continues till all sites become stable ($h_{i,j} < h_{th}$ for all (i, j)). When toppling occurs at the boundary of the lattice, extra heights get off the lattice and are removed from the system. With continuous addition of unit height (sand grain) at random sites of the lattice, the avalanches (toppling) get correlated over longer and longer ranges and the average height (h_{av}) of the system grows with time. Gradually the correlation length (ξ) becomes of the order the system size L as the system attains the critical average height $h_c(L)$. On average, the additional height units start leaving the system and the average height remains stable there (see Fig. 12 (a)). The distributions of the avalanche sizes and the corresponding life times follow robust power laws [17], hence the system becomes critical here.

We can perform a finite size scaling fit $h_c(L) = h_c(\infty) + CL^{-1/\nu}$ (by setting $\xi \sim |h_c(L) - h_c(\infty)|^{-\nu} = L$), where C is a constant, with $\nu \simeq 1.0$ gives $h_c \equiv h_c(\infty) \simeq 2.124$ (see inset of Fig. 12 (a)). Similar finite size scaling fit with $\nu = 1.0$ gave $h_c(\infty) \simeq 2.124$ in earlier large scale simulations [16].

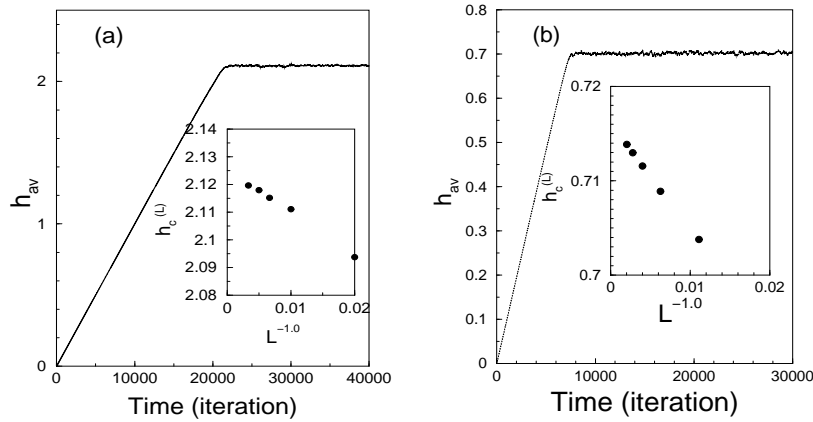


Fig. 12: Growth of BTW (a) and Manna (b) sandpiles. Inset shows the system size dependence of the critical height.

Manna proposed the stochastic sand-pile model [16] by introducing randomness in the dynamics of sand-pile growth in two-dimensions. Here, the critical height is 2. Therefore at each toppling, two rejected grains choose their host among the four available neighbours randomly with equal probability. After constant adding of sand grains, the system ultimately settles at a critical state having height h_c . A similar finite size scaling fit $h_c(L) = h_c(\infty) + CL^{-1/\nu}$ gives $\nu \simeq 1.0$ and $h_c \equiv h_c(\infty) \simeq 0.716$ (see inset of Fig. 12 (b)). This is close to an earlier estimate $h_c \simeq 0.71695$ [19], made in a somewhat different version of the model. The avalanche size distribution has got power laws similar to the BTW model, however the exponent seems to be different [16, 17], compared to that of BTW model.

Sub-critical response: Precursors

We are going to investigate the behavior of BTW and Manna sandpiles when they are away from the critical state ($h < h_c$). At an average height h_{av} , when all sites of the system have become stable (dynamics have stopped), a fixed number of height units h_p (pulse of sand grains) is added at any central point of the system [8, 18]. Just after this addition, the local dynamics starts and it takes a finite time or iterations to return back to the stable state ($h_{i,j} < h_{th}$ for all (i, j)) after several toppling events. We measure the response parameters: $\Delta \rightarrow$ number of toppling $\tau \rightarrow$ number of iteration and $\xi \rightarrow$ correlation length which is the distance of the furthest toppled site from the site where h_p has been dropped.

(A) In BTW model

We choose $h_p = 4$ for BTW model to ensure toppling at the target site. We found that all the response parameters follow power law as h_c is approached: $\Delta \propto (h_c - h_{av})^{-\lambda}$, $\tau \propto (h_c - h_{av})^{-\mu}$, $\xi \propto (h_c - h_{av})^{-\nu}$; $\lambda \cong 2.0$, $\mu \cong 1.2$ and $\nu \cong 1.0$. Now if we plot $\Delta^{-1/\lambda}$, $\tau^{-1/\mu}$ and $\xi^{-1/\nu}$ with h_{av} all the curve follow straight line and they should touch the x axis at $h_{av} = h_c$. Therefore by a proper extrapolation we can estimate the value of h_c and we found $h_c = 2.13 \pm .01$ (Fig. 13) which agree well with direct estimates of the same.

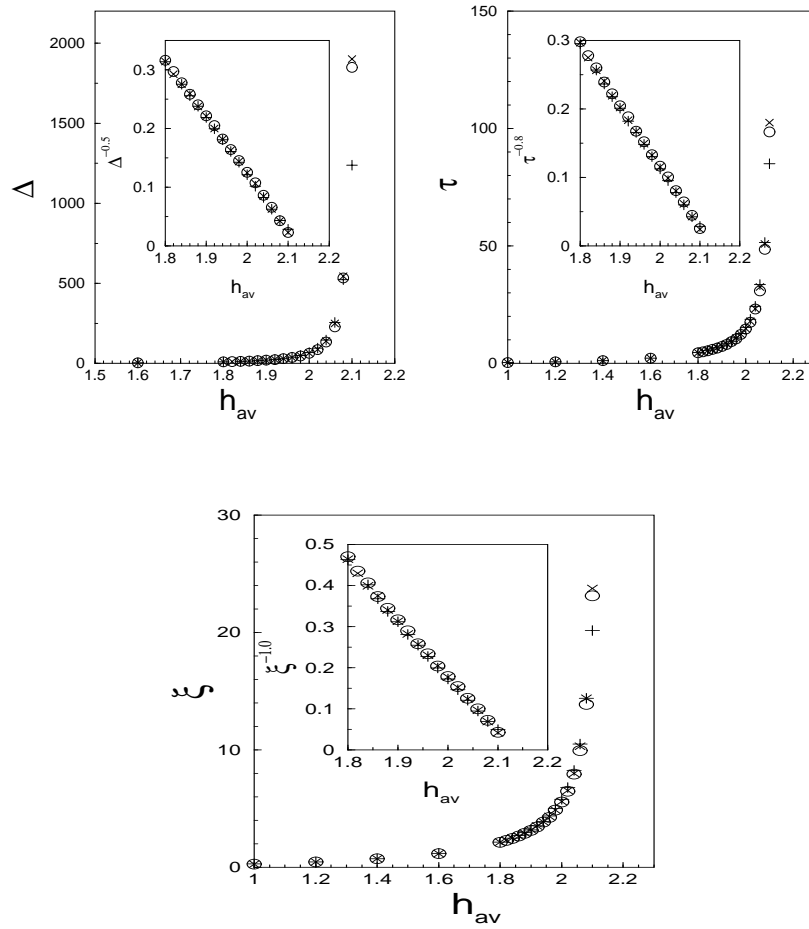


Fig. 13: Precursor parameters and prediction of critical point in BTW model.

(B) In Manna model

Obviously we have to choose $h_p = 2$ for Manna model to ensure toppling at the target site. Then we measured all the response parameters and they seem to follow power law as h_c is approached: $\Delta \propto (h_c - h_{av})^{-\lambda}$, $\tau \propto (h_c - h_{av})^{-\mu}$, $\xi \propto (h_c - h_{av})^{-\nu}$; $\lambda \cong 2.0$, $\mu \cong 1.2$ and $\nu \cong 1.0$. As in BTW model, all the curve follow straight line if we plot $\Delta^{-1/\lambda}$, $\tau^{-1/\mu}$ and $\xi^{-1/\nu}$ with h_{av} and proper extrapolations estimate the value of $h_c = 0.72 \pm .01$ which is again a good estimate (Fig. 14).

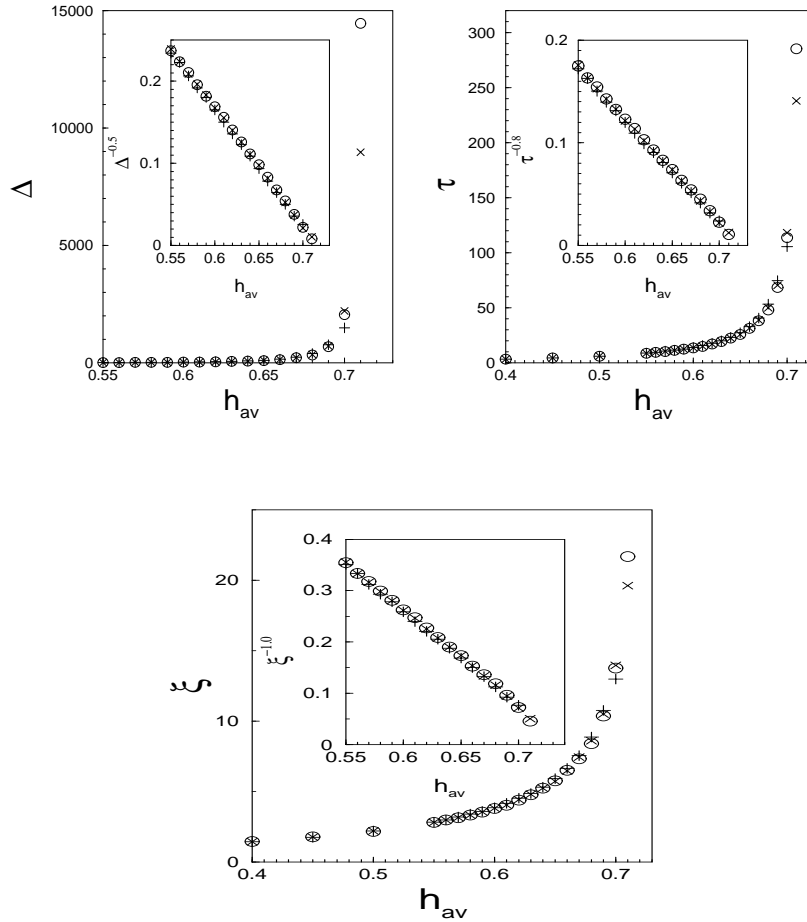


Fig. 14: Precursor parameters and prediction of critical point in Manna model.

Our simulation results suggest that although BTW and Manna models belong to different universality class with respect to their properties at the

critical state, both the models show similar sub-critical response or precursors. A proper extrapolation method can estimate the respective critical heights of the models quite accurately.

2.4 Fractal overlap model of earthquake

It has been claimed recently that since the fractured surfaces have got well-characterized self-affine properties, the distribution of the elastic energies released during the slips between two fractal surfaces (earthquake events) may follow the overlap distribution of two self-similar fractal surfaces [20, 21, 22, 23]. To support this idea, Chakrabarti and Stinchcombe [24] have analytically shown using renormalization group technique that for regular fractal overlap (Cantor sets and carpets) the contact area distribution follows power law. This claim has also been verified by extensive numerical simulations [25]. If one cantor set moves uniformly over other, the overlap between the two fractals (Fig. 15) change quasi-randomly with time. In this section we analyse the time series data of such overlaps to find the prediction possibility of a next large overlap.

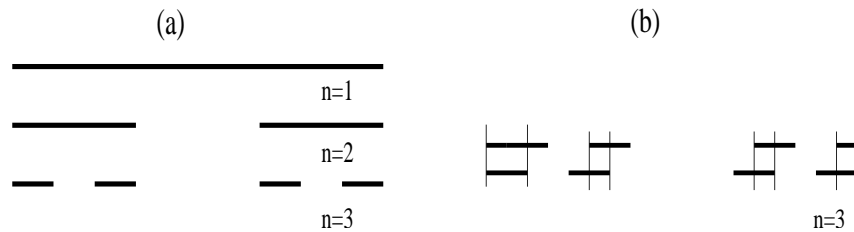


Fig. 15: (a) A regular Cantor set of dimension $\ln 2 / \ln 3$; only three finite generations are shown. (b) The overlap of two identical (regular) Cantor sets, at $n = 3$, when one slips over other; the overlap sets are indicated within the vertical lines, where periodic boundary condition has been used.

The time series data analysis

We consider now the time series obtained by counting the overlaps $m(t)$ as a function of time as one Cantor set moves over the other (periodic boundary condition is assumed) with uniform velocity. The time series are shown in Fig. 16., for finite generations of Cantor sets of dimensions $\ln 2 / \ln 3$ and $\ln 4 / \ln 5$ respectively.

We calculate the cumulative overlap size $Q(t) = \int_0^t m dt$. We see that ‘on average’ $Q(t)$ is seen to grow linearly with time t for regular Cantor sets. This gives a clue that instead of looking at the individual overlaps $m(t)$ series one may look for the cumulative quantity. In fact, for the regular Cantor set of dimension $\ln 2 / \ln 3$, the overlap m is always 2^k , where k is an integer.

However the cumulative $Q(t) = \sum_{i=0}^t 2^{k_i}$ can not be easily expressed as any simple function of t . Still, we observe $Q(t) \simeq ct$, where c is dependent on M .

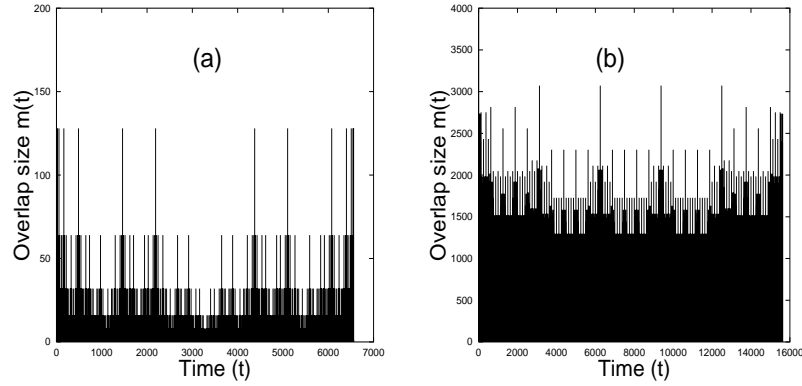


Fig. 16: The time (t) series data of overlap size (m) for regular Cantor sets: (a) of dimension $\ln 2/\ln 3$, at 8th generation: (b) of dimension $\ln 4/\ln 5$, at 6th generation.

We first identify the ‘large events’ occurring at time t_i in the $m(t)$ series, where $m(t_i) \geq M$, a pre-assigned number. Then, we look for the cumulative overlap size $Q(t) = \int_{t_i}^{t_{i+1}} m dt$, where the successive large events occur at times t_i and t_{i+1} . The behavior of Q_i with time is shown in Fig. 17 for regular cantor sets with $d_f = \ln 2/\ln 3$ at generation $n = 8$. Similar results are also given for Cantor sets with $d_f = \ln 4/\ln 5$ at generation $n = 6$ in Fig. 18. It appears that there are discrete (quantum) values up to which Q_i grows with time t and then drops to zero value.

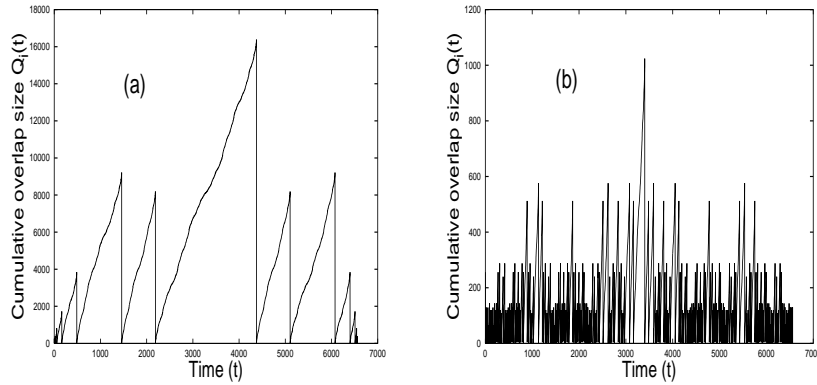


Fig. 17: The cumulative overlap size variation with time (for regular Cantor sets of dimension $\ln 2/\ln 3$, at 8th generation), where the cumulative overlap has been reset to 0 value after every big event (of overlap size $\geq M$ where $M = 128$ and 32 respectively).

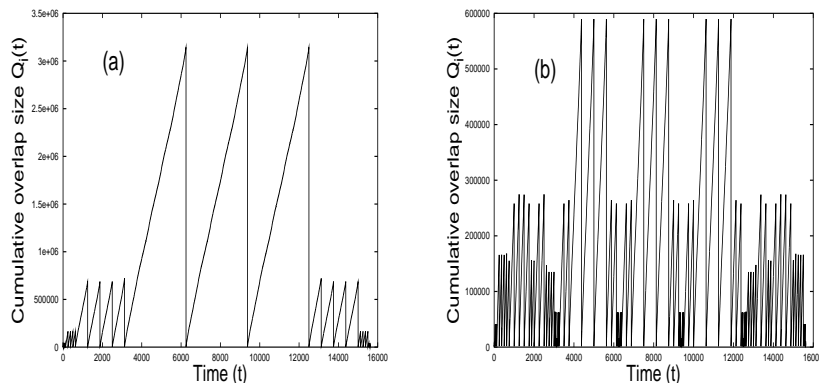


Fig. 18: The cumulative overlap size variation with time (for regular Cantor sets of dimension $\ln 4 / \ln 5$, at 6th generation), where the cumulative overlap has been reset to 0 value after every big event (of overlap size $\geq M$ where $M = 2400$ and 2048 respectively).

Finally we found that if one fixes a magnitude M of the overlap sizes m , so that overlaps with $m \geq M$ are called ‘events’ (or earthquake), then the cumulative overlap Q_i grows linearly with time up to some discrete quanta $Q_i \cong lQ_0$, where Q_0 is the minimal overlap quantum, dependent on M and l is an integer.

3 Conclusions

Knowledge of precursors sometimes help to estimate precisely the location of the global failure or critical point through a proper extrapolation procedure. Therefore precursors which are available long before the global failure, can be used to resist an imminent global failure.

In all the dynamical systems studied here, we find that long before the occurrence of global failure, the growing correlations in the dynamics of constituent elements manifest themselves as various precursors. In Fiber Bundle Model, the breakdown susceptibility χ and the relaxation time τ , both diverge as the external load or stress approaches the global failure point or critical point. The distribution of avalanches exhibits a crossover in power law exponent values when the system comes closer to the failure point. Also the pattern of inclusive avalanches can tell us whether a bundle can support the applied load or not. In Fuse model, divergence of susceptibility and crossover in avalanche power law exponent are the signature of imminent breakdown of the system. Whereas in both BTW and Manna sandpile models the number of toppling Δ , relaxation time τ and the correlation length ξ grow and diverge following power laws as the systems approach their respective critical points h_c from the sub-critical states. Therefore these parameters directly help to predict the critical point in advance. However in fractal overlap model the time series data analysis suggest that the cumulative overlap sizes can assume

some quantized values which indirectly helps to speculate whether a large overlap (event) is imminent or not.

Acknowledgment: S. P. thanks the Research Council of Norway (NFR) for financial support through Grant No. 166720/V30.

References

1. B. K. Chakrabarti and L. G. Benguigui, *Statistical Physics of Fracture and Breakdown in Disorder Systems*, Oxford Univ. Press, Oxford (1997); H. J. Herrmann and S. Roux (Eds), *Statistical Models for the Fracture of Disordered Media*, North Holland, Amsterdam (1990); P. Bak, *How Nature Works*, Oxford Univ. Press, Oxford (1997).
2. F. T. Peirce, *J. Textile Inst.* **17**, T355-368 (1926).
3. H. E. Daniels, *Proc. R. Soc. London A* **183** 405 (1945).
4. P. C. Hemmer and A. Hansen, *J. Appl. Mech.* **59** 909 (1992); A. Hansen and P. C. Hemmer, *Phys. Lett. A* **184** 394 (1994); M. Kloster, A. Hansen and P. C. Hemmer, *Phys. Rev. E* **56** 2615 (1997).
5. S. Pradhan, A. Hansen and P. C. Hemmer, *Phys. Rev. Lett.* **95** 125501 (2005); S. Pradhan and A. Hansen, *Phys. Rev. E* **72** 026111 (2005).
6. D. Sornette, *J. Phys. A* **22** L243 (1989); D. Sornette, *J. Phys. I (France)* **2** 2089 (1992); A. T. Bernardes and J. G. Moreira, *Phys. Rev. B* **49** 15035 (1994).
7. S. Zapperi, P. Ray, H. E. Stanley and A. Vespignani, *Phys. Rev. Lett.* **78** 1408 (1997); Y. Moreno, J. B. Gomez and A. F. Pacheco, *Phys. Rev. Lett.* **85** 2865 (2000).
8. S. Pradhan and B. K. Chakrabarti, *Phys. Rev. E* **65**, 016113 (2001);
9. S. Pradhan, P. Bhattacharyya and B. K. Chakrabarti, *Phys. Rev. E* **66**, 016116 (2002);
10. P. Bhattacharyya, S. Pradhan and B. K. Chakrabarti, *Phys. Rev. E* **67**, 046122 (2003);
11. A. Hansen and P. C. Hemmer, *Trends Stat. Phys.* **1** 213 (1994). R. C. Hidalgo, F. Kun and H. J. Herrmann, *Phys. Rev. E* **64** 066122 (2001); S. Pradhan, B. K. Chakrabarti and A. Hansen, *Phys. Rev. E* **71** 036149 (2005).
12. B. D. Coleman, *J. Appl. Phys.* **27**, 862 (1956); B. D. Coleman, *Trans. Soc. Rheol.* **1**, 153 (1957); B. D. Coleman, *Trans. Soc. Rheol.* **2**, 195 (1958).
13. S. L. Phoenix, *SIAM (Soc. Ind. Appl. Math.) J. Appl. Math.* **34**, 227 (1978); S. Roux, *Phys. Rev. E* **62**, 6164 (2000); R. Scorretti, S. Ciliberto and A. Guarino, *Europhys. Lett.* **55**, 626 (2001).
14. S. Pradhan and B. K. Chakrabarti, *Phys. Rev. E* **67**, 046124 (2003).
15. P. Bak, C. Tang and K. Wiesenfeld, *Phys. Rev. Lett.* **59** 381 (1987); P. Bak, C. Tang and K. Wiesenfeld, *Phys. Rev. A* **38** 364 (1988).
16. S. S. Manna, *J. Stat. Phys.* **59** 509 (1990); P. Grassberger and S. S. Manna, *J. Phys. France* **51** 1077 (1990); S. S. Manna, *J. Phys. A: Math. Gen.* **24** L363 (1991).
17. D. Dhar, *Physica A* **270** 69 (1999); D. Dhar, *Physica A* **186** 82 (1992); D. Dhar, *Physica A* **263** 4 (1999).

18. M. Acharyya and B. K. Chakrabarti, *Physica A* **224** 254 (1996); *Phys. Rev. E* **53** 140 (1996).
19. A. Vespignani, R. Dickman, M. A. Munoz and S. Zapperi, *Phys. Rev. E* **62** 4564 (2000); A. Chessa, E. Marinari and A. Vespignani, *Phys. Rev. Lett.* **80** 4217 (1998).
20. Gutenberg, B. and Richter, C. F., *Seismicity of the Earth and Associated phenomena*, Princeton University Press, Princeton, N.J. (1954).
21. R. Burridge, L. Knopoff, *Bull. Seis. Soc. Am.* **57** 341 (1967).
22. J. M. Carlson, J. S. Langer, *Phys. Rev. Lett.* **62** 2632. (1989)
23. V. De Rubeis et al, *Phys. Lett.* **76** 2599 (1996).
24. B. K. Chakrabarti, R. B. Stinchcombe, *Physica A* **270** 27 (1999).
25. S. Pradhan, B. K. Chakrabarti, P. Ray and M. K. Dey, *Phys. Scr. T* **106** 77 (2003); S. Pradhan, P. Chaudhuri and B. K. Chakrabarti, in *Continuum Models and Discrete Systems*, Ed. D. Bergman, E. Inan, Nato Sc, Series, Kluwer Academic Publishers (Dordrecht) 245 (2004).